Flow Field Analysis in Vortex Ring State using Small Diameter Rotor by Descent Simulation

Ryuki Mori[1], Ayato Takii[1,2], Masashi Yamakawa[1], Yusei Kobayashi[1], Shinichi Asao[3] and Seiichi Takeuchi[3]

1 Kyoto Institute of Technology, Matsugasaki, Sakyo-ku, Kyoto 606-8585, Japan
m3623032@edu.kit.ac.jp
2 RIKEN Center for Computational Science, 7-1-26 Minatojima-minami-machi, Chuo-ku, Kobe 650-0047, Hyogo, Japan
3 College of Industrial Technology, 1-27-1, Amagasaki 661-0047, Hyogo, Japan

Abstract. While the unstable turbulence condition known as Vortex Ring State in rotorcraft has been studied mainly in helicopters, there have not been many studies of drones, which have become more active in recent years. In particular, there are few studies using numerical simulations focusing on small diameter rotors such as quadcopters. In this paper, descent simulations are performed using a rotor model with a diameter of 8 inches and a propeller pitch of 4.5 inches, which is used for quadcopters. In this study, Moving Computational Domain method is used to reproduce the descent motion of the rotor over the entire moving computational domain. In addition, Sliding mesh method is applied to reproduce the rotor rotation within the computational grid. This method allows flow field analysis under free rigid body motion of the analytical model. The displacement of the computational domain itself is applied at each step to reproduce the descent conditions. By combining these methods, fluid flow simulations under vertical descent and conditions are performed to visualize the flow field. Flow field evaluation using the Q criterion showed that even in a small rotor, circulating vortices are generated at a velocity close to the induced velocity v_h. VRS was also observed around the rotor under the conditions of horizontal speed $V_H = 2.0v_h$, $descent\ speed\ V_Y = 1.0v_h$, and descent angle of 26.6 deg, but at the same time vortex divergence was also observed. It was inferred that the forward velocity component helps to avoid Vortex Ring State.

Keywords: VRS (Vortex Ring State), CFD, quadcopter, small propeller

1 Introduction

Helicopters and other rotorcrafts enter an unstable state called Vortex Ring State (VRS) by descending vertically or nearly vertically at a speed close to the rotor wake velocity (induced speed). VRS is a very unstable and turbulent state, characterized by the formation of a toroidal vortex around the main rotor. At the same time, during VRS, wake dominates the inflow region of the rotor during descent, reducing the blade angle of

ICCS Camera Ready Version 2024
To cite this paper please use the final published version:
DOI: 10.1007/978-3-031-63749-0_7

attack and causing thrust loss and thrust oscillations at the mean thrust value [1, 2]. This instability causes the rotorcraft to oscillate and crash due to significant changes in thrust and attitude angle. Once the rotor enters the VRS, it is difficult to predict the motion of the rotorcraft, so it is important to avoid the VRS. Therefore, various studies on rotors have been conducted.

Efimov (2022) et al. investigated VRS in a single rotor in a wind tunnel test and found that thrust is regained when the angle between the axis of rotation of the propeller and the air velocity vector exceeds 40 deg [3]. Wind tunnel tests using Particle Image Velocimetry (PIV) revealed that the vortex core exists in the upper and lower regions of the rotor surface and that the vortex moves freely from its development to its extinction [4]. Due to experimental cost challenges and advances in numerical computation, many numerical simulations have investigated the VRS characteristics of rotors. Stalewski (2020) et al. performed unsteady calculations of the flow field in the VRS by coupling the URANS equation with the helicopter's equation of motion and found qualitative agreement for both experimental studies and flight tests [5]. There have also been many studies, both experimental and simulation, on how to avoid VRS. It was found that VRS cannot occur at all descent speeds when the angle of descent is minimal, such as below 30 deg, by reducing the accumulation of rotor wake by forward speed [6]. Furthermore, it was also found that the aircraft does not enter VRS when the angle of descent is less than 20 deg [3].

Drones are another rotary-wing aircraft that has become increasingly active in recent years. They are used for a variety of purposes, including industrial monitoring, observation of damage in disaster areas, and video production. Quadcopters, one type of drone, like other rotary-wing aircraft, are also subject to VRS during descent, so attention has been focused on safety during flight.

To study VRS in quadcopters, numerical simulations focusing on aerodynamic interference between rotors during descent were performed using the RANS equation [7]. Further numerical calculations were performed using the Open FOAM CFD package, and a method was proposed to detect VRS by differential pressure measurements when given various descent rates [8].

Actually, however, among rotary-wing aircraft, VRS has been investigated mainly for helicopters, and few studies have focused on quadcopters. Furthermore, there are only a few VRS studies that utilize CFD focusing on the small-diameter rotor portion represented by these aircraft. In addition, there are still few studies that consider the effect of the rotor model's own motion on the VRS in the flow field simulation of VRS research. The reason is that realizing this numerical simulation involves a very complex moving boundary problem, which makes it difficult to combine the interaction with fluid dynamics, which deals with the flow around the model.

And most of these studies are based on steady-state wind tunnel testing and CFD. However, as a practical phenomenon, VRS is unstable and transient. Therefore, the authors propose a method that combines the MCD (Moving Computational Domain) method [9], which is based on the unstructured mesh finite volume method [10,11], and the sliding mesh method [12]. MCD method is good at discretizing a 4-dimensional inspection volume by applying the finite volume method to it and performing calculations that strictly satisfy geometric conservation laws. Furthermore, sliding mesh

ICCS Camera Ready Version 2024
To cite this paper please use the final published version:
DOI: 10.1007/978-3-031-63749-0_7

method can represent motions such as rotation by forming a computational domain divided by regions with different states of motion and transferring physical quantities at the boundaries of the computational domain. Therefore, this method is considered suitable for general-purpose calculations. Yamakawa et al. (2021) applied this method to investigate the effect of rotating screws on the free surface of water during submarine and other submerged motions [13]. Takii et al. (2020) also applied this technique to the behavior of a tilt-rotor aircraft modeled after the Osprey V-22 in VRS and the surrounding flow field [14]. These results were conducted under the unstructured parallel computational environment [15].

This study focuses on the rotor portion of a quadcopter and simulates the flow field of VRS by solving the unsteady flow during the rotor's descent. For the simulations, unsteady calculations are performed using MCD method based on the unstructured moving mesh finite volume method and the sliding mesh method with the equations of motion of the fluid and the rotational axis motion of the propeller. In order to give different descent velocities to a single rotor, the entire computational domain is subjected to displacements to create a descent condition.

2 Numerical Approach

2.1 Governing Equations

To solve for the flow field around the rotor model, the three-dimensional Euler equations, which are the fundamental equations for inviscid compressible fluids, are used as governing equations. The equations in conserved form, after non-dimensionalization, are written as follows:

$$\frac{\partial \boldsymbol{q}}{\partial t}+\frac{\partial \boldsymbol{E}}{\partial x}+\frac{\partial \boldsymbol{F}}{\partial y}+\frac{\partial \boldsymbol{G}}{\partial z}=0, \tag{1}$$

$$\boldsymbol{q}=\begin{pmatrix}\rho\\ \rho u\\ \rho v\\ \rho w\\ e\end{pmatrix}, \boldsymbol{E}=\begin{pmatrix}\rho u\\ \rho u^2+p\\ \rho uv\\ \rho uw\\ u(e+p)\end{pmatrix}, \boldsymbol{F}=\begin{pmatrix}\rho v\\ \rho uv\\ \rho v^2+p\\ \rho vw\\ v(e+p)\end{pmatrix}, \boldsymbol{G}=\begin{pmatrix}\rho w\\ \rho uw\\ \rho vv\\ \rho w^2+p\\ w(e+p)\end{pmatrix} \tag{2}$$

where $\boldsymbol{q}$ is the conserved quantity vector, and $\boldsymbol{E}, \boldsymbol{F}, \boldsymbol{G}$ are the flux vector. Furthermore ρ is the density of the fluid, u, v, w are the x, y, z components of velocity, respectively, and e is the total energy per unit volume. The pressure p is determined by the ideal gas equation of state shown below, assuming that the fluid to be handled is an ideal gas:

$$p=(\gamma-1)\left[e-\frac{1}{2}\rho(u^2+v^2+w^2)\right] \tag{3}$$

where the specific heat ratio is assumed to be $\gamma = 1.4$. In a computational environment, the Reynolds number is approximately 3,400,000 and the maximum Mach number is 0.136.

ICCS Camera Ready Version 2024
To cite this paper please use the final published version:
DOI: 10.1007/978-3-031-63749-0_7

2.2 Unstructured Moving-Grid Finite-Volume Method

Unstructured Moving-Grid Finite-Volume Method is used for calculations that involve moving and deforming the computational grid. In this method, the flux is evaluated on a 4-dimensional (x, y, z, t) inspection volume so that the geometric conservation law (GCL) [16] is satisfied. Applying Gauss' divergence theorem to the 4-dimensional inspection volume, the 3-dimensional Euler equations are transformed as follows:

$$\begin{aligned}\int_{\Omega}\left(\frac{\partial \boldsymbol{q}}{\partial t}+\frac{\partial \boldsymbol{E}}{\partial x}+\frac{\partial \boldsymbol{F}}{\partial y}+\frac{\partial \boldsymbol{G}}{\partial z}\right)d\Omega &= \int_{\Omega}(\boldsymbol{E},\boldsymbol{F},\boldsymbol{G},\boldsymbol{q})\cdot\tilde{n}\,dV \\ &= \sum_{l=1}^{6}\left(\boldsymbol{E}\widetilde{n_x}+\boldsymbol{F}\widetilde{n_y}+\boldsymbol{G}\widetilde{n_z}+\boldsymbol{q}\widetilde{n_t}\right)_t = 0\end{aligned} \tag{4}$$

where Ω is the inspection volume, $\tilde{\boldsymbol{n}} = \left(\widetilde{n_x}, \widetilde{n_y}, \widetilde{n_z}, \widetilde{n_t}\right)$ is the outward unit normal vector on $\partial\Omega$, l is the surface number of the inspection volume.

2.3 Moving Computational Domain Method

This paper calculates the flow field generated during the descent of a quadcopter rotor. Conventional CFD is an alternative to wind tunnel testing, in which a stationary model is subjected to flow and the flow around it is calculated. In the MCD method, the entire computational domain moves with the objects in the domain, as shown in Fig. 1.

The fluid flow around the object is generated by the movement of the boundary surface. In order to handle flows with no known inflow or outflow, this study deals with moving boundaries by applying a far-field boundary condition in which the inflow and outflow are determined by Riemann invariants. Furthermore, the rotor model is free to move with the computational domain, regardless of the size of the computational grid, since this method eliminates the limitation of computational space. By combining the MCD method with the sliding mesh method, this method is also applicable to rotor rotation.

Flow variables are defined at the cell centers of the unstructured mesh. The flux vectors are evaluated using the Roe flux difference separation method [17]. The vanLeer-like restriction function proposed by Hishida et al. is used with respect to the physical quantity gradient of each cell [18]. This reconstructs the solution and extrapolates the cell boundary values to a higher order to achieve higher spatial accuracy. Then, a two-stage rational Runge-Kutta method is used to perform pseudo-temporal progression.

ICCS Camera Ready Version 2024
To cite this paper please use the final published version:
DOI: 10.1007/978-3-031-63749-0_7

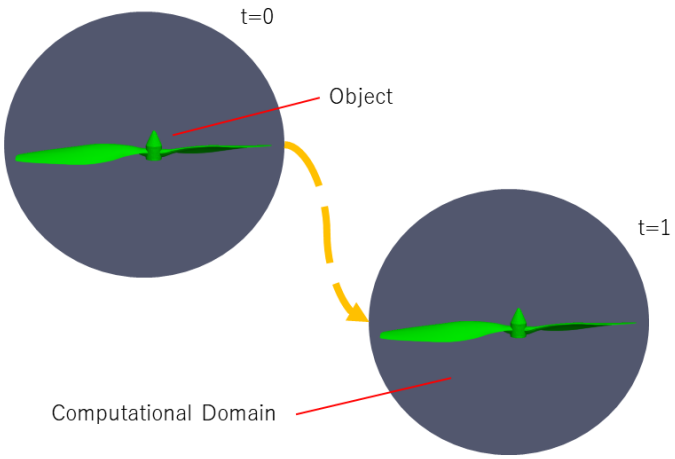

Fig. 1. Moving Computational Domain Method

The sliding mesh method [19] is also applied to reproduce the rotation of the rotor model in the computational domain by transferring physical quantities. This method allows the mesh itself to slide at specific boundaries, deforming the mesh while maintaining its volume.

In this study, the sliding mesh method is used only for the axis of rotation because of the rotor alone.

2.4 Hovering Induced Velocity

VRS is considered to occur when a rotorcraft descends at a speed close to its hovering induced velocity v_h, which is given by momentum theory in the following equation [7].

$$v_h = \sqrt{\frac{T_0}{2\rho A_b}} \tag{5}$$

where T_0 is the rotor thrust [N] during hovering, ρ is the density [kg/m^3], and A_b is the rotor blade area [m^2]. In this case, a quadcopter propeller model was used. The weight of the quadcopter model is $M = 0.9721$ kg, and the total force of all rotors is obtained from the equation of the balance of force with gravity. Then, by dividing by the number of rotors, the force T_0 is derived as follows:

$$T_0 = \frac{Mg}{N_{rotor}} \tag{6}$$

where $N_{rotor} = 4$ is the number of rotors in a rotorcraft and $g = 9.80665$ m/s^2 is the gravitational acceleration constant. In this study, the conditions for VRS generation are set by giving the descent velocity based on the hovering induced velocity $v_h = 5.253$ m/s for the rotor model.

ICCS Camera Ready Version 2024
To cite this paper please use the final published version:
DOI: 10.1007/978-3-031-63749-0_7

3 Descent Simulation of rotor

3.1 Computational Mesh

The rotor model used in this study is modeled after the propeller of a commercial quadcopter drone, DJI's Flame Wheel ARF KIT F450, shown in Fig. 2. Table 1 shows the various parameters of the propeller model.

Table 1. Specifications of the computational model

Rotor Size	8 inches (0.203 m)
Blade Pitch	4.5 inches (0.114 m)
Number of Rotor Blades	2
Hovering Rotor Rotation Speed	4214 rpm
Direction of Rotation	Counter Clockwise

Fig. 2. F450 quadcopter

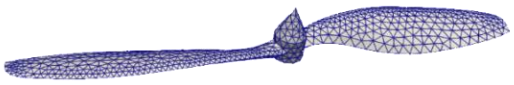

Fig. 3. Computational surface grid

The computational domain consists of two regions separated by a sliding mesh. The first is a cylindrical region that encompasses the rotor model, and the second is a spherical region that encompasses the cylindrical region. The cylindrical part has a sliding mesh structure as shown in Fig. 4, and is used to propagate physical quantities. The computational grid was created by MEGG3D software [20,21] and consists of a tetrahedral lattice. The number of lattices in the entire computational domain is 684,965. The number of lattices and minimum lattice width of the rotor model are 177,385 and 0.008 (4.8 mm), respectively.

Fig. 5 shows a cross-sectional view of the entire computational domain and a grid cross-section around the rotor model. The rotor length and the radius of the spherical computational domain are 0.2778L and 50L, respectively, for a representative length L=0.60 m for the entire quadcopter length.

ICCS Camera Ready Version 2024
To cite this paper please use the final published version:
DOI: 10.1007/978-3-031-63749-0_7

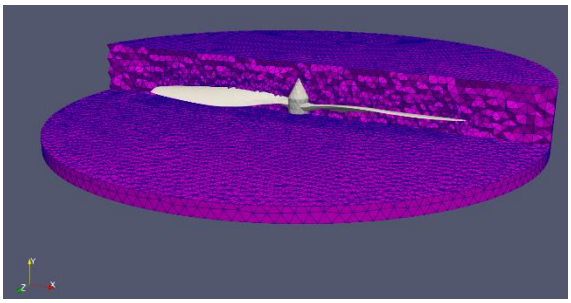

Fig. 4. Sliding mesh domain

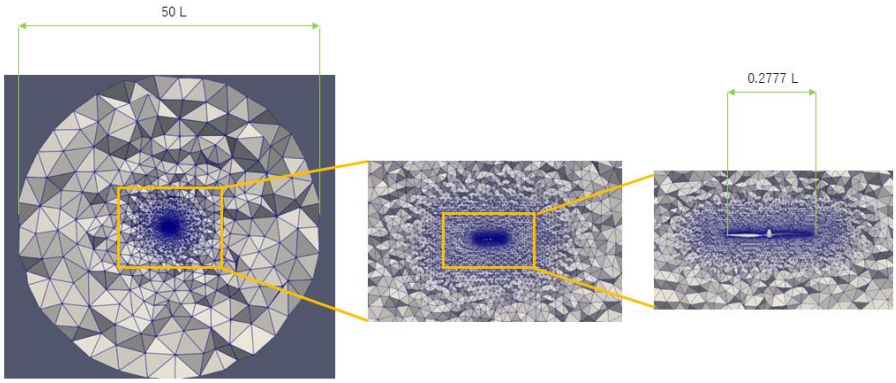

Fig. 5. Computational Domain

3.2 Computational Mesh

In this study, the descent state is reproduced by applying a displacement in the negative Y-axis direction at each step over the entire computational domain that encompasses the rotor model. Furthermore, the computational domain performs a descent motion with constant velocity. Therefore, the model motion does not depend on the translational and rotational equations of motion, but only on the following equations:

$$\boldsymbol{r}(\boldsymbol{n}+\boldsymbol{1}) = \frac{\boldsymbol{dr}}{\boldsymbol{dt}}\Delta t + \boldsymbol{r}(n) \tag{7}$$

where $\boldsymbol{r}(n)$ is the position vector of the model center at step n and Δt is the time tick width.

Rotor rotation rises with equal acceleration from 0 to 5000 steps from the stop condition to the target speed of 4214 rpm at the same time as the descent condition. After reaching the target rpm, the rotor continues to rotate at a constant speed.

Table 2 shows the initial and boundary conditions for the variables. The representative velocity and density are calculated to be 340.29 m/s and 1.247 kg/m^3, respectively. The variables are also non-dimensionalized by these representative values.

ICCS Camera Ready Version 2024
To cite this paper please use the final published version:
DOI: 10.1007/978-3-031-63749-0_7

Table 2. Initial condition and Boundary condition

ρ	1
p	1.0/γ
u, v, w	0
Rotor Surface	Slip wall condition
Outer Boundary	Riemann invariant boundary condition

4 Numerical Simulation Results

4.1 Simple vertical descent

This section presents the results of a vertical descent simulation for a rotor model with descent velocities $V_Y = 0.4v_h, V_Y = 0.9v_h$, respectively. The output results are visualized using Paraview [16]. The graph is a csv file converted from the output file using the standard Paraview method "CellDatatoPointData". A positive value of Q criterion is used in the output figure. This is the second invariant of the velocity gradient tensor and helps identify regions in the flow field where rotation is more dominant than strain.

Fig. 6 shows contour plots of the Q criterion for $V_Y = 0.4v_h, V_Y = 0.9v_h$, respectively, together with the velocity vector in the Y direction. When $V_Y = 0.4v_h$, most of the vortex portion stays at a position lower than the rotor surface. After a while, it is seen that the vortex region is pushed further down the rotor due to the downwash effect. In addition, focusing on the velocity vector in the Y direction, a large vortex flow can be seen below the rotor surface. On the other hand, when $V_Y = 0.9v_h$, the vortex area stays at the same or higher position than the rotor surface. This is thought to be because the rotor is descending at the same rate as the downwash. The vortex is expected to continue to stay at the rotor surface. The magnitude of the Q criterion is also large near the rotor surface for $V_Y = 0.9v_h$. The Y-directional velocity vector shows the flow circulating at a height close to the rotor surface.

Fig. 7 shows the isosurfaces at Q criterion = 0.05 for $V_Y = 0.4v_h, V_Y = 0.9v_h$ respectively. At $V_Y = 0.4v_h$, the vortex is strongly affected by downwash with time and moves away from the rotor surface. At $V_Y = 0.9v_h$, a toroidal shape of Q criterion isosurface is seen covering the rotor surface for almost the entire time period. The descending motion close to the induced velocity confirms the characteristics of the VRS, in which the wake of the rotor circulates around the rotor surface.

ICCS Camera Ready Version 2024
To cite this paper please use the final published version:
DOI: 10.1007/978-3-031-63749-0_7

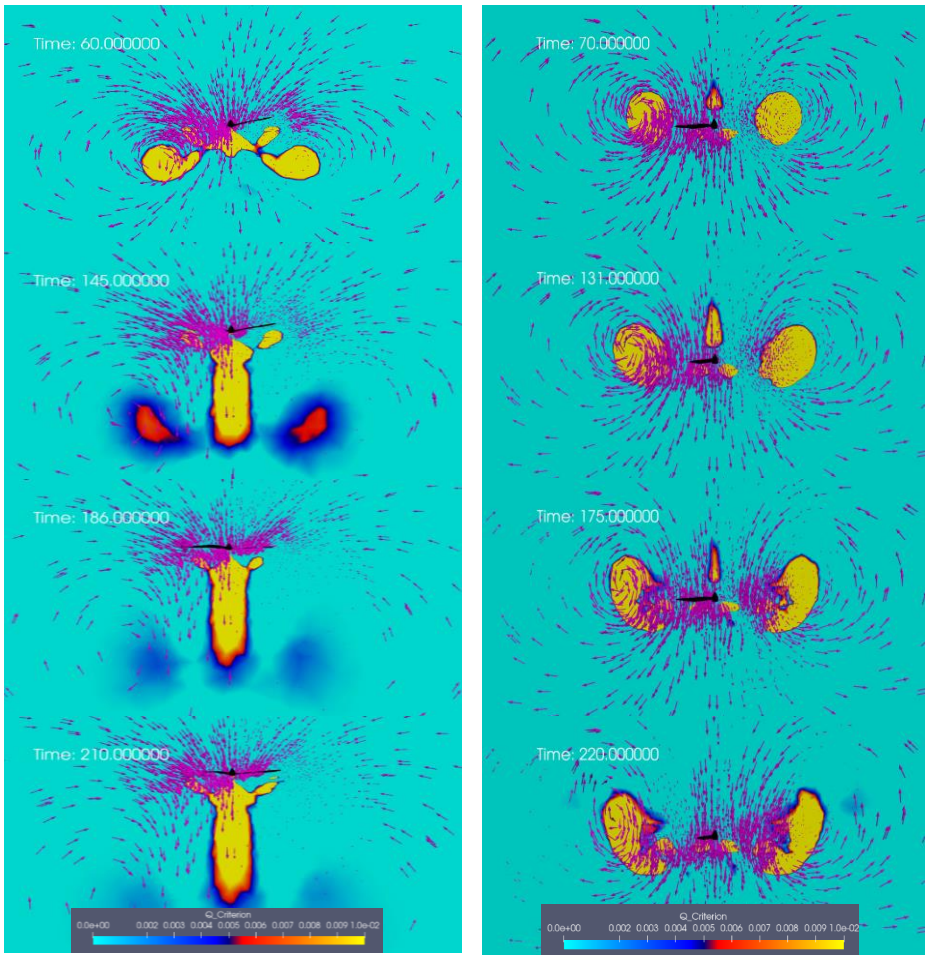

(a) $V_Y = 0.4v_h$ (b) $V_Y = 0.9v_h$

Fig. 6. Q criterion contour map with velocity vector in Y direction

ICCS Camera Ready Version 2024
To cite this paper please use the final published version:
DOI: 10.1007/978-3-031-63749-0_7

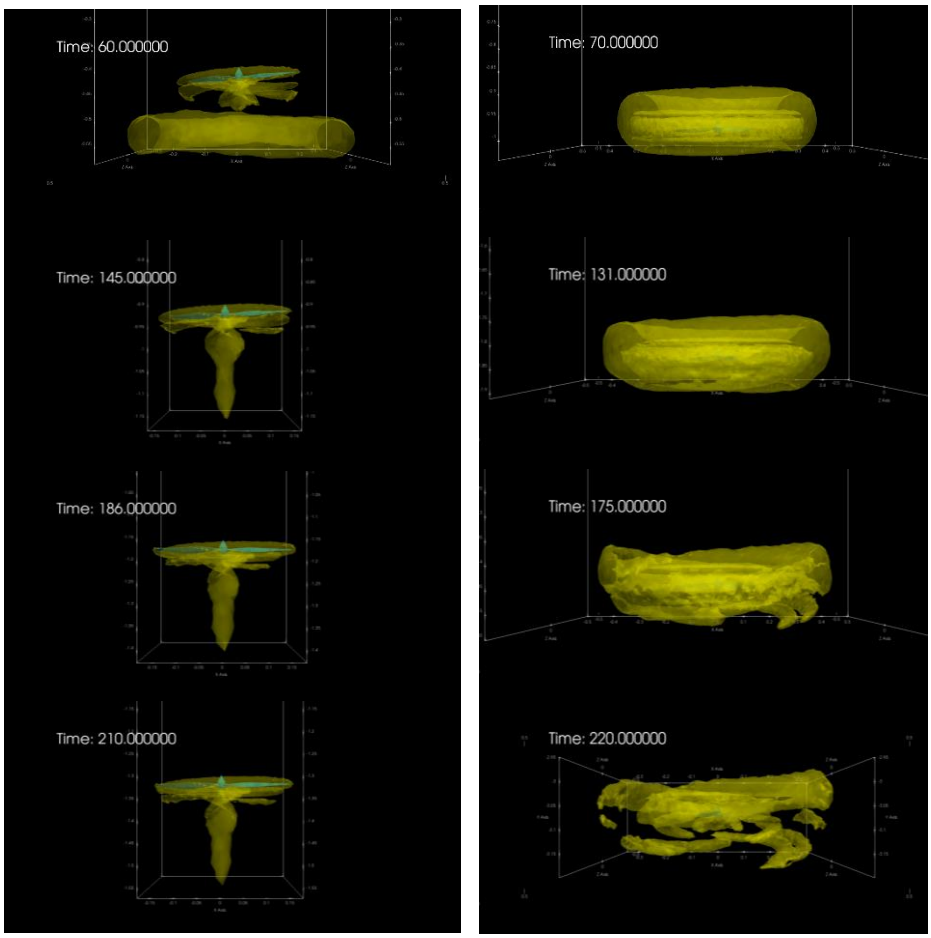

(a) $V_Y = 0.4v_h$ (b) $V_Y = 0.9v_h$

Fig. 7. Isosurfaces with Q criterion=0.05

4.2 Oblique Descent Simulation (angle of descent 26.6 deg)

This section shows the results of a descent simulation for the rotor model with descent conditions $V_H = 2.0v_h, V_Y = 1.0v_h$ (angle of descent 26.6 deg).

Fig. 8 shows the contour plot of the Q criterion at $V_H = 2.0v_h, V_Y = 1.0v_h$, together with the velocity vector in the Y direction. The rotor is moving toward the lower left in the figure, and it can be seen that the vortex portion is also stagnant at approximately the same position as the rotor surface, as it was at $V_Y = 0.9v_h$. This may be due to the fact that the descent velocity V_Y is about the same as the hovering induced velocity v_h. Furthermore, due to the rotor's own horizontal velocity motion, it tries to move away from the vortex relatively. This tendency is expected to continue. However, the vortex is generally dominant at the top of the rotor, and a VRS may be detected.

ICCS Camera Ready Version 2024
To cite this paper please use the final published version:
DOI: 10.1007/978-3-031-63749-0_7

Fig. 9 shows the isosurface for Q criterion=0.05. As with $V_Y = 0.9v_h$, there is vortex stagnation at the rotor surface over each time step. However, the vortex region is swept in the opposite direction of descent by the forward velocity, confirming that it is diverging.

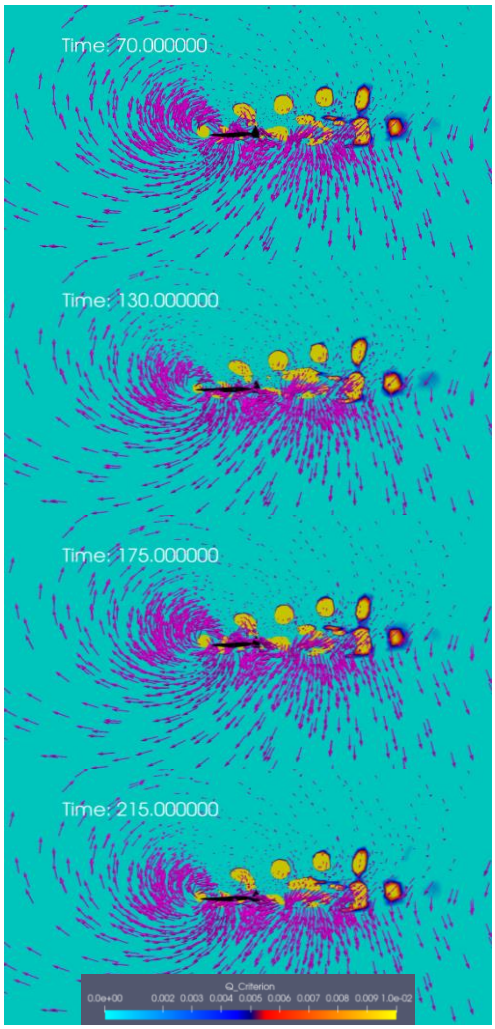

Fig. 8. Q criterion contour map with velocity vector in Y direction ($At\ V_H = 2.0v_h, V_Y = 1.0v_h$)

ICCS Camera Ready Version 2024
To cite this paper please use the final published version:
DOI: 10.1007/978-3-031-63749-0_7

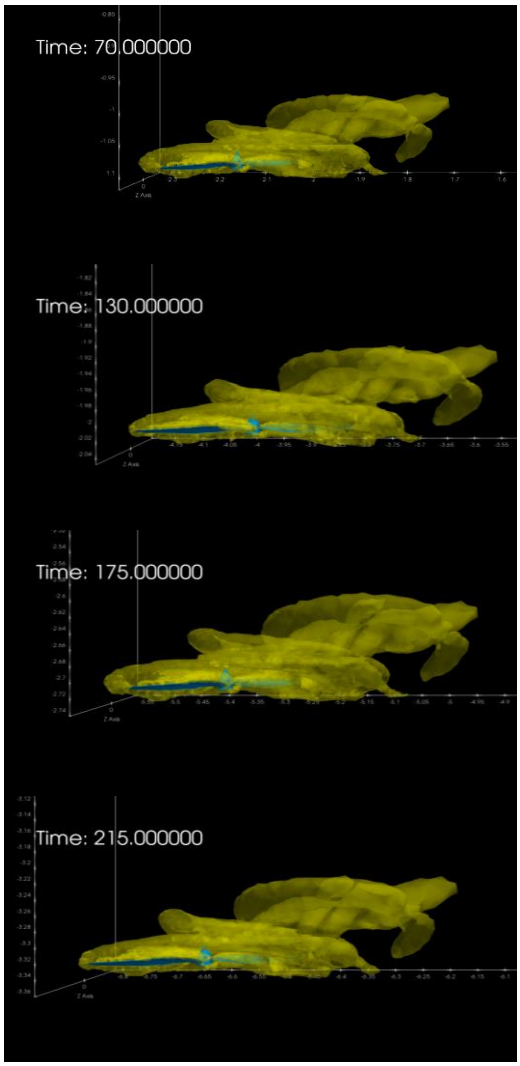

Fig. 9. Isosurfaces with Q criterion=0.05 ($At\ V_H = 2.0v_h, V_Y = 1.0v_h$)

5 Conclusions

Descent simulations were performed to investigate the unsteady state for the VRS of a single small diameter rotor. In this study, the MCD method based on the unstructured moving mesh finite volume method and the sliding mesh method were used. The MCD method is based on the unstructured moving mesh finite volume method, and the sliding mesh method is based on the unstructured moving mesh finite volume method. The descent simulations were performed for a simple vertical descent with

ICCS Camera Ready Version 2024
To cite this paper please use the final published version:
DOI: 10.1007/978-3-031-63749-0_7

$V_Y = 0.4, v_h,\ V_Y = 0.9v_h$ and a descent with $V_H = 2.0v_h, V_Y = 1.0v_h$ at a descent angle of 26.6 deg.

By evaluating the flow field around the rotor during descent, the nature of VRS as an unsteady phenomenon was reaffirmed. The flow field evaluation was visualized using Q criterion contour plots. In the simple vertical descent, when $V_Y = 0.9v_h$, the rotor model descends at the same speed as the downwash, and it was confirmed that the vortex stays around the rotor surface. This indicates that even small-diameter rotors can fall into VRS, a result that is qualitatively consistent with previous studies. Simulations were also conducted under the descent conditions of $V_H = 2.0v_h, V_Y = 1.0v_h$ at a descent angle of 26.6 deg. In this case, vortex retention was observed, but due to the forward velocity component, the flow behind the rotor was observed to flow in the opposite direction of the flight direction. This suggests that VRS may be avoided under descent conditions with a constant angle of descent by promoting the divergence of the vortex due to the forward velocity, which is in accordance with previous VRS research. In actual flight, however, the pitch angle is expected to increase as the attitude angle of the rotor. Since this point was not taken into account in this study, it needs to be reviewed.

Based on the single-rotor simulations in this study, we would like to extend the study to quadcopters equipped with the rotor model used in this study in the future and conduct VRS avoidance research. In addition, this method restricted the equation of motion of the rigid body to the rotor model, thereby providing arbitrary descent conditions. Therefore, we would like to evaluate the trajectory and attitude angle of the quadcopter using a 6-DOF coupled flight simulation that combines the equations of the fluid and rigid body.

References

1. A. Brand, M. Dreier, R. Kisor and T. Wood.: The Nature of Vortex Ring State. In: AHS 63rd Annual Forum, Virginia Beach, USA (2007)
2. M. D. Betzina.: Tiltrotor Descent Aerodynamics: A Small-Scale Experimental Investigation of Vortex Ring State. In: AHS 57th Annual Forum, Washington, USA (2001)
3. Vadim V. Efimov, Konstantin O. Chernigin.: Vortex ring state as a cause of a single-rotor helicopter unanticipated yaw. In: Aerospace Systems, Volume 5, pp. 413–418 (2022)
4. K. Surmacz, P. Ruchała, W. Stryczniewicz.: Wind tunnel tests of the development and demise of Vortex Ring State of the rotor. In: Advances in Mechanics: Theoretical, Computational and Interdisciplinary Issues, pp. 551-554 (2016)
5. Wienczyslaw Stalewski, Katarzyna Surmacz.: Investigations of the vortex ring state on a helicopter main rotor based on computational methodology using URANS solver. In: MATEC Web Conf, 9th EASN International Conference on “Innovation in Aviation & Space”, Volume 304 (2019)
6. S. Taamallah.: A Qualitative Introduction to the Vortex-Ring-State, Autorotation, and Optimal Autorotation. In: Nationaal Lucht- en Ruimtevaartlaboratorium National Aerospace Laboratory NLR, 36th European Rotorcraft Forum, Paris, France (2010)
7. Junjie Wang, Renliang Chen, Jiaxin Lu and Yanqin Zhao.: Numerical simulation of the quadcopter flow field in the vertical descent state. In: Proc IMechE Part G, J Aerospace Engineering 2022, Vol. 0(0) 1–13, (2022)

ICCS Camera Ready Version 2024
To cite this paper please use the final published version:
DOI: 10.1007/978-3-031-63749-0_7

8. Joel McQuaid, Amir Kolaei, Ph.D., Götz Bramesfeld, Ph.D. , Paul Walsh, Ph.D.: EARLY ON-SET PREDICTION OF VORTEX-RING STATE OF QUADROTORS. In: Journal of Aerospace Engineering, Volume 33, Issue 6 (2020)
9. Yamakawa, M. et al.:Numerical Simulation of Rotation of Intermeshing Rotors using Added and Eliminated Mesh Method, Procedia Computer Science, Volume 108, pp.1883-1892(2017)
10. Yamakawa, M. et al.:Numerical Simulation for a Flow around Body Ejection using an Axisymmetric Unstructured Moving Grid Method, Computational Thermal Sciences, Vol.4, No.3, pp.217-223(2012)
11. Yamakawa, M. et al.:Optimization of knee joint maximum angle on dolphin kick, Physics of Fluids, Volume 32, Issue 61, Article number 067105, (2020)
12. Takii, A. et al.:Six Degrees of Freedom Numerical Simulation of Tilt-Rotor Plane, Lecture Notes in Computer Scienc, Volume 11536 LNCS, pp.506-519(2019)
13. Yamakawa, M., Yoshioka, K., Asao, S., Takeuchi, S., Kitagawa, A., Tajiri, K.: Numerical simulation of free surface affected by submarine with a rotating screw moving underwater. In: Paszynski, M., Kranzlmüller, D., Krzhizhanovskaya, V.V., Dongarra, J.J., Sloot, P.M.A. (eds.) ICCS 2021. LNCS, vol. 12747, pp. 268–281. Springer, Cham (2021)
14. Ayato Takii, Masashi Yamakawa, and Shinichi Asao.: Descending Flight Simulation of Tiltrotor Aircraft at Different Descent Rates. Springer Nature Switzerland AG 2020 V. V. Krzhizhanovskaya et al. (Eds.): ICCS (2020), LNCS 12143, pp. 178–190, 2020. https://doi.org/10.1007/978-3-030-50436-6_13
15. Yamakawa, M. et al.:Domain decomposition method for unstructured meshes in an OpenMP computing environment, Computers & Fluids, Vol. 45, pp.168-171(2011)
16. Roe, P.L.: Approximate Riemann solvers, parameter vectors, and diference schemes. In: J. Comput. Phys. 43(2), pp.357–372 (1981)
17. Hishida, M., et al.: A new slope limiter for fast unstructured CFD solver FaSTAR. In: Proceedings of 42nd Fluid Dynamics Conference/Aerospace Numerical Simulation Symposium. Japan Aerospace Exploration Agency, JAXA-SP-10-012, pp. 85–90 (in Japanese) (2010)
18. Takii, Ayato, Masashi Yamakawa, Shinichi Asao, and Kyohei Tajiri.: Six degrees of freedom flight simulation of tilt-rotor aircraft with nacelle conversion. In: Journal of Computational Science 44 (2020): 101164.
19. Ito, Y., et al.: Surface triangulation for polygonal models based on CAD data. Int. J. Numer. Methods Fluids 39(1), 75–96 (2002)
20. Ito, Y.: Challenges in unstructured mesh generation for practical and efficient computational fluid dynamics simulations. Comput. Fluids 85(1), 47–52 (2013)
21. Paraview Homepage, https://www.paraview.org/, last accessed 2024/2/25

ICCS Camera Ready Version 2024
To cite this paper please use the final published version:
DOI: 10.1007/978-3-031-63749-0_7